Am J Transl Res 2019;11(1):393-405
www.ajtr.org /ISSN:1943-8141/AJTR0082169

Original Article

NUP58 facilitates metastasis and epithelial-mesenchymal transition of lung adenocarcinoma via the GSK-3β/Snail signaling pathway

Jianlin Shi[1*], Chen Li[3*], Hui Wang[2], Benshan Xiao[4], Wanfang Qiu[5]

Departments of [1]Thoracic Surgery, [2]Gastroenterology, Yan'an Affiliated Hospital of Kunming Medical University, 245 East Renmin Road, Kunming 650051, China; [3]The First Affiliated Hospital of Kunming Medical University, 295 Xichang Road, Kunming 650032, China; [4]Department of Thoracic Surgery, Jiujiang University Clinical Medical College, 57 East Xunyang Road, Jiujiang 332000, China; [5]Department of Cell Biology and Medical Genetics, Kunming Medical University, Kunming 650050, China. [*]Equal contributors.

Received July 5, 2018; Accepted December 23, 2018; Epub January 15, 2019; Published January 30, 2019

Abstract: The NUP58 gene encodes a nucleus-pore protein that is a component of nuclear pore complex (NPC). NPC facilitates the transportation of macromolecules (ions and other substances) into the nuclei of eukaryotic cells. However, there are no relevant reports about the NUP58 gene in human lung cancer. In this study, we demonstrated that NUP58 was highly expressed in the primary and metastatic foci of lung adenocarcinoma, with low expression in adjacent tissues and normal lung tissue. In patients with lung adenocarcinoma, the NUP58 gene was highly expressed in patients with stage IV disease ($P < 0.05$); NUP58 knockdown using a lentiviral vector-mediated shRNA inhibited metastasis and invasion of lung adenocarcinoma cell lines A549 and H1299 in vivo and in vitro. Furthermore, silencing of NUP58 resulted in altered expression of EMT markers, associated GSK-3β/Snail pathways, tumor metastasis and invasion factors. In conclusion, these findings demonstrated that NUP58 can promote the metastasis and invasion of lung adenocarcinoma, which can be partially attributed to the GSK-3β/Snail signaling pathway.

Keywords: NUP58, EMT, lung adenocarcinoma, metastatic mechanism

Introduction

Recently, the global cancer population has soared as a result of environmental pollution, smoking and other adverse factors, among which the morbidity and mortality of lung cancer remain the highest in global malignancies [1]. In China, the morbidity of lung cancer is increasing year by year, and the annual growth rate is 1.63% [2], of which approximately 85% of cases are non-small cell lung cancer (NSCLC) [3]. Although great progress has been made in the diagnosis and treatment of malignant tumors, 90% of deaths among patients with advanced cancer can be attributed to metastasis [4]. The prognosis of lung cancer has not been radically improved because of our limited understanding of multiple-step metastasis and a lack of effective measures.

As early as 1889, Paget [5] proposed the theory of "seed and soil" for tumor metastasis. Tumor cells are the equivalent of "seed", and the microenvironment of the metastasis is the "soil". Subsequent studies have confirmed that tumor metastasis involves local invasion of primary tumor cells into surrounding tissues, intravasation of tumors cells into blood vessels or lymphatic drainages, survival in the circulatory system, extravasation through blood vessels and colonization at distant parts of the body [6]. Current major molecular mechanisms for tumor metastasis include: 1. Epithelial-mesenchymal transition (EMT). 2. Circulating tumor cells (CTCs). 3. Metastatic colonization; and 4. Metastatic microenvironment [4]. Epithelial-mesenchymal transition refers to the cellular process by which cells gain mesenchymal traits and lose epithelial traits. This process plays an

important role in embryonic development, chronic inflammation, tissue remolding, tumor metastasis and other pathological processes [7]. Some pathological factors, including hypoxia or certain factors in tumor microenvironment (TGF-β, FGF, EGF, HGF, Wnt, Notch, Hedgehog), and their associated signaling pathways (MAPK, PI3K, NF-κB, Wnt/β-catenin, Notch) can directly or indirectly induce epithelial-mesenchymal transition [8]. There are two main changes in EMT: 1). Cytological changes including loss of epithelial cell adhesion and cell polarity; 2). Molecular changes including reduction of epithelial proteins (E-cadherin, claudins and cytokeratin) and increases in interstitial protein (N-cadherin, fibronectin and vimentin) [9]. With these changes, tumor cells gain stronger invasive and migratory abilities [10]. EMT-induced transcription factors have been found in a variety of tumors and include Snail, Slug, Twist, TCF4, ZEB1 and FOXC2 [11].

The NUP58 gene encodes a nucleus-pore protein that is a component of the nuclear pore complex (NPC). NPC facilitates the transportation of macromolecules (ions and other substances) into the nuclei of eukaryotic cells [12]. The NUP58 gene has been reported in colorectal cancer cell lines (DLD1 and SW480), and after RNA interference is introduced, the cell viability is decreased, suggesting that NUP58 may become a target for colorectal cancer treatment [13]. In addition, the NUP58 gene was also found in MDCK cell lines (a cell model for studying cell polarity and epithelial cell morphogenesis), which showed that the cell polarity disappeared after RNA interference treatment, suggesting that NUP58 gene could promote cell morphogenesis [14]. Previously, we screened the NUP58 gene for lung cancer metastasis using bioinformatics and a wound-healing assay (Supplementary Figure 1). There are no relevant reports about the NUP58 gene in lung cancers. Therefore, using in vitro and in vivo approaches, we investigated whether NUP58 plays a role in the metastasis of human lung cancer cells and its mechanisms.

Materials and methods

Cell lines and culture

The human NSCLC cell lines H1299, A549, 95D and H1975 used in this study were obtained from the ATCC in 2010. All of the cell lines were routinely cultured at 37°C in a humidified air atmosphere containing 5% carbon dioxide in F12K or 1640 supplemented with 10% FBS (Biowest), 100 m/mL penicillin (Sigma-Aldrich), and 100 mg/mL streptomycin (Sigma-Aldrich). All cell lines were used within 20 passages and thawed fresh every 2 months. These cell lines were mycoplasma-free and authenticated by quality examinations of morphology and growth profile.

Human adenocarcinoma samples

Two cohorts of tissue microarrays were purchased from Shanghai Outdo Biotech Co., Ltd., China. One microarray contained 92-paired human lung adenocarcinomas and their matched adjacent noncancerous tissues (Supplementary Table 2). The other microarray contained 36-paired human lung adenocarcinomas and their matched adjacent noncancerous tissues (the positive and negative lymph nodes were all included). The matched adjacent noncancerous samples were taken at a distance of at least 3 cm from the tumor. Upon resection, human surgical specimens were immediately frozen in liquid nitrogen and stored in a -80°C freezer for further investigation. All human specimens were approved by the Ethical Review Committee of the World Health Organization of the Collaborating Center for Research in Human Production authorized by the Shanghai Municipal Government and obtained with informed consent from all patients. This study was approved by the Ethics Committee of Kunming Medical University.

Immunohistochemical (IHC) staining

Paraffin blocks were sectioned to a thickness of 4 mm. The wax was melted at 63°C overnight. The sections were deparaffinized in xylene, rehydrated in graded alcohol series and boiled in 0.01 M citrate buffer (pH 6.0) for 2 min in an autoclave. Endogenous peroxidase activity was blocked using hydrogen peroxide (0.3%), which was followed by incubation with 5% bovine serum albumin to reduce nonspecific binding. Tissue sections were incubated with an anti-NUP58 rabbit polyclonal antibody (1:500 dilution) (HPA039360, Sigma). The slides were rinsed with PBS and a secondary antibody (rabbit) was applied at a 1:500 dilution in PBS for 30 minutes at room temperature. After rinses with PBS for 30 s, the slides were incubated

with streptavidin-HRP for 30 min at room temperature and then rinsed with PBS and incubated for 15 min with the chromogen 3,3-diaminobenzidine and counterstained with hematoxylin. The slides were then examined under a transmission light microscope. The cytoplasmic staining of NUP58 in tumor tissue was scored by a semiquantitative method as reported previously [15]. The percentage of positive cells in cytoplasm was scored as follows: grade 0 (absent or < 1%), grade 1 (1-25%), grade 2 (26-50%), grade 3 (51-75%), and grade 4 (76-100%). The staining intensity was also graded (0, 1+, 2+, 3+). The immunoreactivity score was determined by multiplying the intensity score by the percentage of positive cells. The IS range was from 0-12. The cutoff threshold for this scoring system was set to 8 and a score of ≥ 8 was considered as high NUP58 expression and < 8 as low NUP58 expression.

Transduction of lung adenocarcinoma cells with shRNA

Lentiviral constructs expressing NUP58 shRNA (NUP58-shRNA-LV) were purchased from Shanghai Genechem Co., Ltd., China. The NUP58 shRNA vector sequence was as follows: 5'-ACAGGATTTACTCTAAATA-3'. The sequence of a nonspecific control siRNA was 5'-TTCTCCGAACGTGTCACGT-3'. A549 and H1299 cells were seeded in 6-well plates at a concentration of 2.0 * 10^5 cells per well (20-30% confluence) on the day before shRNA transduction. NUP58-shRNA-LV was transduced into cells at a multiplicity of infection (MOI) of 10 (A549) or 5 (H1299) using polybrene (8 μg/ml) and Enhanced Infection Solution (Genechem, China). At the same time, a nontarget negative control virus GFP-LV (Genechem, China) was transduced into cells using the same methods to control for the impact of the viral vector. After incubation for 12 h, the medium was replaced with fresh medium. Transduction effects were observed with a fluorescence microscopy camera 72 h after transduction. The cells were harvested for mRNA and protein analysis as well as other assays at the indicated time points.

Wound-healing assay

Cell migration was evaluated using the Oris™ plate (Platypus Technology, USA). Briefly, the cells were collected and seeded into 96-well plates at the appropriate concentration (3-5 * 10^4/well). The seeded plates containing the Oris™ Pro Biocompatible Gel were incubated in a humidified chamber (37°C, 5% CO_2) for 24 hours (cell line dependent) to permit cell attachment. The next day, the plates were removed from the incubator, and the inserts were removed from the wells. After the wells were washed with serum-free medium, low serum medium (0.5% FBS) was added to the wells. The cells were examined using an imaging instrument throughout the incubation period to monitor the progression of migration. Post-migration images of the detection zone were captured using fluorescence microscopy (0 h, 8 h, 16 h, and 24 h) according to the cell type. The experiments were repeated independently three times.

Cell migration and invasion assay

The migration assay was performed with transwell inserts that had 6.5-mm polycarbonate membranes and pores 8.0 μm in size (Corning Inc., NY, USA). Briefly, 1 * 10^5 cells were resuspended in serum-free medium and added to the upper chamber. Culture medium containing 10% FBS was used as a chemoattractant in the lower chamber. The cells were incubated for 18 h in a humidified incubator at 37°C. The cells that migrated through the membrane pores to the lower surface of the membrane were fixed and stained with crystal violet. Stained cells in each field were photographed, and the number of stained cells per chamber was counted in six randomly selected fields. Each experiment was performed in triplicate.

Affymetrix gene expression profile and IPA analysis

Total RNA from cells (shNUP58 A549 and shCtrl A459) was analyzed using Agilent 2100. The qualified RNA samples were generated to aRNA (amplified RNA) by GeneChip3' IVT Express Kit (i.e., through single chain synthesis of cDNA, further through the two-chain synthesis of a two-stranded DNA template, and then through in vitro inversion of aRNA with biotin markers). The aRNA was purified and then segmented and crossed with the chip probes. After the hybridization was finished, the chips were dyed and finally scanned for pictures and raw data.

RT-qPCR

Total RNA from cells was isolated using Trizol as recommended by the manufacturer (TAKARA, Dalian, China). The concentration and purity of the total RNA were assessed using a UV spectrophotometer (Nanodrop2000/2000c, Thermo). Total RNA was reverse-transcribed using the Promega M-MLV Reagent kit (Promega Beijing, China). Quantitative PCR (qPCR) was performed with the CFX96™ Real-Time System (Bio-Rad, USA) using the SYBR Master Mixture (TAKARA, Dalian, China). The primers are listed in Supplementary Table 1. GAPDH was used as an internal control. The relative expression levels of mRNAs were calculated using the $2^{\Delta Ct}$ method, where ΔCt = Ct of objective gene -Ct of GAPDH, and then transformed to log2. Each reaction was repeated independently at least three times.

Western blotting

Cells were washed twice with ice-cold phosphate-buffered saline (PBS), and cellular protein was extracted using RIPA buffer (10 mM Tris, pH 7.5, 0.1 M NaCl, 1 mM EDTA, and 0.1% Triton X-100). The protein preparation was subjected to 12% sodium dodecyl sulfate-polyacrylamide gel electrophoresis (SDS-PAGE), and electro-transferred to a nitrocellulose membrane (Millipore, MA). The membranes were blocked with TBST buffer (20 mM Tris, pH 7.5, 500 mM NaCl, 0.05% Tween-20, and 0.2% Triton X-100) containing 5% skim milk, then incubated with the primary antibodies against different proteins at 4°C overnight, followed by incubation with a secondary antibody. Bands were visualized by ECL and a TM Western blotting system (Amersham). The antibodies used in Western blotting analysis included anti-NUP58 (HPA039360, Sigma), anti-E-cadherin (#3195, CST), anti-N-cadherin (#4061, CST), anti-GAPDH (SC-32233, Santa Cruz), anti-vimentin (AB92547, abcam), anti-Snail (#3879, CST), anti-Twist (AB49254, abcam), anti-GSK-3β (#9325, CST), and anti-GSK-3β (ser9) (#5558, CST). Original western blot images are shown in Supplementary Figure 3.

Protocols and animals

Five-week-old female BALB/c nude mice were obtained from the Shanghai Lingchang company. These mice were maintained in a specific pathogen-free unit under isothermal conditions. All of the experimental procedures were conducted in accordance with the Institutional Animal Committee of Kunming Medical University. A549 cells ($2.0 * 10^7$/mL) transduced with NUP58 shRNA or negative control vector were suspended in 100 μl of PBS. The cells were then injected into the tail vein of nude mice to form xenograft tumors. After approximately 57 days, all mice received injections of D-luciferin (15 mg/mL) into their abdominal cavities. After 15 minutes, 10 μl/g of 0.7% pentobarbital sodium anesthesia was intraperitoneally administered to each animal. Mice were placed in a live imaging apparatus for imaging and observation of fluorescence. When the imaging was complete, the mice were injected with an overdose of 2% pentobarbital sodium (0.5 mL) for euthanasia, and death was confirmed after a complete coma and dislocation of the cervical spine. Medical scissors and medical tweezers were used to dissect animals and to observe their lungs and livers to identify metastasis. All data were preserved.

Cancer Genome Atlas data analysis

Gene expression data from 546 samples (488 tumors and 58 matched noncancerous tissues) from lung adenocarcinomas and clinical data were downloaded from The Cancer Genome Atlas (TCGA, http://cancergenome.nih.gov, RNA-Seq Version 2). Statistical analyses were performed using R software (V3.0.3) (http://www.R-project.org/). *P* values less than 0.05 were considered statistically significant.

Statistical analysis

All data are displayed as the mean ± standard deviation (SD) and were analyzed using one-way ANOVA and Student's t-tests as appropriate and processed using the statistical software SPSS 17.0 and GraphPad Prism (7.01). The differences in NUP58 expression between tumor and normal tissues were tested using nonparametric Kruskal-Wallis analysis. *P* values less than 0.05 were considered significant. All experiments were repeated in triplicate.

Results

Expression of NUP58 in lung adenocarcinomas and cell lines

NUP58 protein levels were examined in two independent cohorts (92-paired and 36-paired

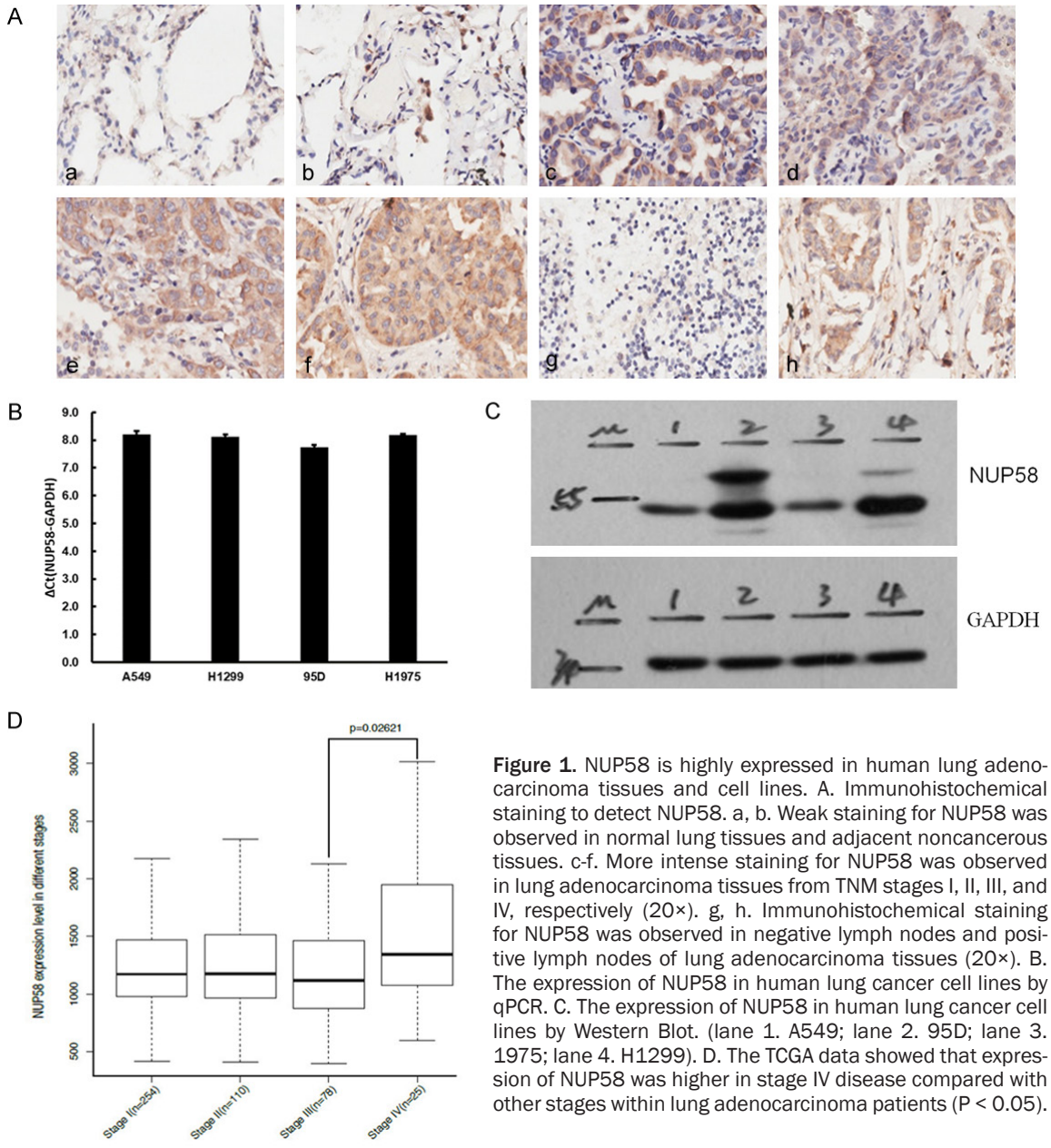

Figure 1. NUP58 is highly expressed in human lung adenocarcinoma tissues and cell lines. A. Immunohistochemical staining to detect NUP58. a, b. Weak staining for NUP58 was observed in normal lung tissues and adjacent noncancerous tissues. c-f. More intense staining for NUP58 was observed in lung adenocarcinoma tissues from TNM stages I, II, III, and IV, respectively (20×). g, h. Immunohistochemical staining for NUP58 was observed in negative lymph nodes and positive lymph nodes of lung adenocarcinoma tissues (20×). B. The expression of NUP58 in human lung cancer cell lines by qPCR. C. The expression of NUP58 in human lung cancer cell lines by Western Blot. (lane 1. A549; lane 2. 95D; lane 3. 1975; lane 4. H1299). D. The TCGA data showed that expression of NUP58 was higher in stage IV disease compared with other stages within lung adenocarcinoma patients ($P < 0.05$).

human lung adenocarcinomas and their matched adjacent noncancerous tissues) of human lung adenocarcinoma patients using immunohistochemistry tissue microarray. The results suggested that NUP58 expression was significantly higher in tumor cytoplasm or metastatic lesions than in adjacent tissues or primary lesions ($P < 0.01$; **Figure 1A**; **Tables 1**, **2**). According to qPCR analysis, the expression of NUP58 was higher in the human lung adenocarcinoma cell lines A549, H1299, 95D, and H1975, compares with GAPDH (**Figure 1B**). The protein levels of NUP58 were also identified by Western Blot in the same 4 cell lines (**Figure 1C**). Interestingly, NUP58 expression was higher in the metastatic 95D and H1299 cell lines than in the A549 and 1975 cell lines. Gene expression data from 546 samples (488 tumors and 58 matched noncancerous tissues) from lung adenocarcinomas and clinical data were downloaded from The Cancer Genome Atlas (TCGA, http://cancergenome.nih.gov, RNA-Seq Version 2). Statistical analyses were performed using R software (V3.0.3)

Table 1. Differential expression of NUP58 in cohort 1 tumor samples

Expression of NUP58	Mean ± Std. Deviation	*P* value	Z value
Tumor cytoplasm (n = 92)	7.000 ± 3.483	0.0001	-6.416
Adjacent cytoplasm (n = 88)	3.364 ± 3.035		

Table 2. Differential expression of NUP58 in cohort 2 tumor samples

Expression of NUP58	Mean ± Std. Deviation	*P* value	Z value
Tumor cytoplasm (n = 14)	5.732 ± 2.896	0.005	-2.833
Adjacent cytoplasm (n = 14)	2.286 ± 2.186		
Normal tissues (n = 5)	2.000 ± 1.225	0.067	7.146
Primary lesions (n = 14)	5.732 ± 2.896		
Metastatic lesions (n = 4)	6.625 ± 4.498		
Lymph nodes (n = 13)	4.292 ± 2.675		

(http://www.R-project.org/). The TCGA data showed that expression of NUP58 was higher in stage IV disease than in other stages of lung adenocarcinoma ($P < 0.05$; **Figure 1D**), but the survival analysis did not show a correlation between NUP58 expression and patient survival (Supplementary Figure 2).

Suppression of NUP58 expression using siRNA had significant effects on cell invasion and migration in vitro

To determine the knockdown effects of shRNA lentivirus on NUP58 expression, qPCR and Western Blot were conducted in A549 and H1299 cell lines. The results indicated that the shRNA lentivirus significantly knocked down the expression of NUP58 both at the RNA and protein levels ($P < 0.05$; **Figure 2A**, **2B**). After 3 days of infection with shRNA lentivirus, wound healing and transwell experiments indicated that a significant inhibition of cell invasion was observed in both cell lines treated with NUP58 shRNA compared with the control-treated cells ($P < 0.05$; **Figure 2C-F**).

Suppression of NUP58 using siRNA had significant effects on cell invasion and migration in vivo

To determine the effects of NUP58 on LUAD cell migration and invasion in vivo, the nude mice models were established using shRNA treated A549 cells and control cells. Twenty nude mice were divided into a knockdown group and a negative group.

Results showed that the lung metastasis rate of the NC group was 100% (**Figure 3B**), whereas that of the KD group was 70% (**Figure 3A**). The total number of metastases in the NC group was 450, and the total number of metastases in the KD group was 24 (**Figure 3D**). Liver metastasis in each group was 0% (**Figure 3E**).

Affymetrix gene expression profile and IPA analysis

By comparing the gene chip detection and IPA analysis of A549 cell lines in the KD group and NC group, it was found that the PI3K/AKT signaling pathway in the KD group was significantly inhibited, and the Z-score was -3.207 (**Figure 4A**). Genes NRAS, PIK3R1, NFKBIE, ITGA2, JAK2, NFKB2, NFKB1, PRKCZ, EIF4EBP1, PIK3R3, RRAS2, PPP2R2C, MAP3K8, PTGS2, ITGA4, CXCL5, ATF3, PLAU, RELB, ICAM1, VEGFA, LTB, IL1A, CCL2, IL6, CXCL1, CXCL2, CXCL3, CXCL8, E-cadherin, N-cadherin, Vimentin, Twist, Snail1, and GSK-3β were selected along with the target gene NUP58 for gene network mapping.

NUP58 knockdown downregulated GSK-3β/Snail activity, which is a biomarker of epithelial-mesenchymal transition and PI3K-AKT pathways

By comparing the gene chip detection and IPA analysis of A549 cell lines in the KD group and NC group, it was found that the PI3K-AKT signaling pathway in the KD group was significantly inhibited, and the Z-score was -3.207. Subsequently, qPCR and Western Blot analysis were used to verify that the NRAS, NFKBIE, JAK2, PRKCZ, EIF4EBP1, RRAS2, MAP3K8 and PTGS2 genes in the KD group were all lower than that in the NC group (**Figure 5A**), indicating that they were inhibited ($P < 0.05$). Tumor associated metastasis and invasion factors including ATF3, PLAU, NUP58, RELB, ICAM1, VEGFA, CCL2, IL6, CXCL1, CXCL2, CXCL3, CXCL5, and CXCL8 were expressed to a lower extent in the KD group than in the NC group ($P < 0.05$, **Figure 5B**). EMT markers including N-cadherin, Snail, Twist, GSK-3β, and GSK-3β (ser9) were ex-

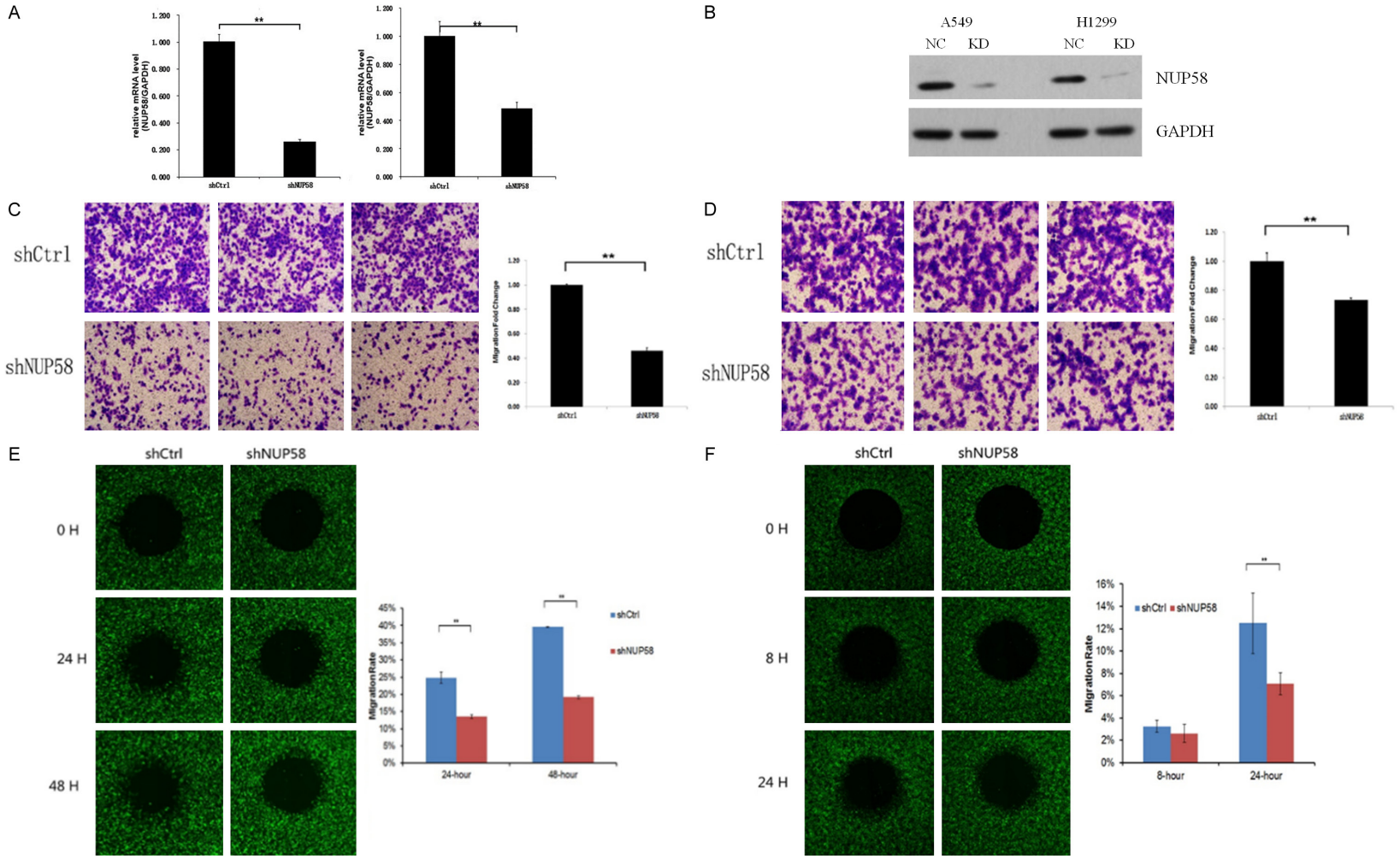

Figure 2. NUP58 enhances A549 and H1299 cell migration and invasion. A and B. A549 and H1299 cells with stable knockdown of NUP58 and its control were identified and analyzed by qPCR. C and D. The cell images (magnification, 100×) of wound-healing assay. The relative cell migrated area at each time point compared with time 0 h was measured using ImageJ software. The mean value (± SD) of three independent experiments is shown; **indicates statistical significance ($P < 0.01$). E and F. The images (magnification, 100×) of cells that migrated into plate wells (lower chamber) in the transwell migration assay. The number of migrated cells was counted by ImageJ software. The mean value (± SD) of three independent experiments is shown; **indicates statistical significance ($P < 0.01$).

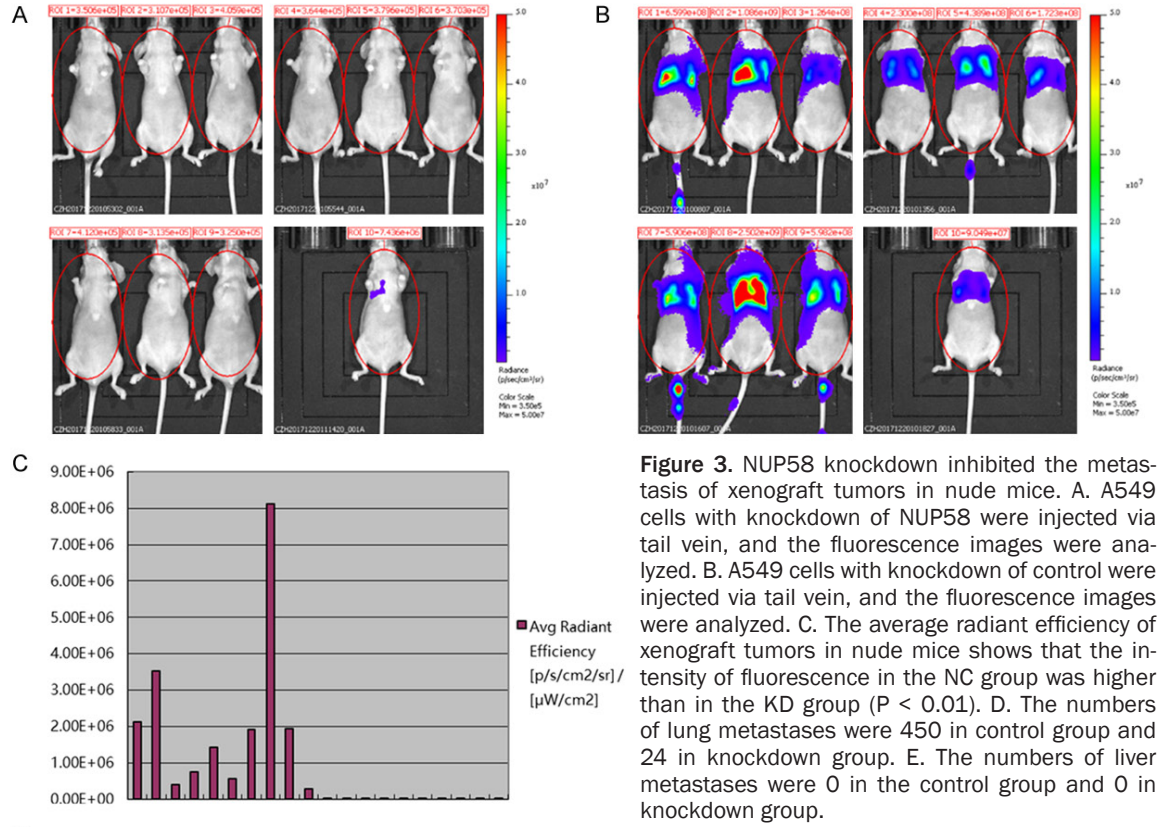

Figure 3. NUP58 knockdown inhibited the metastasis of xenograft tumors in nude mice. A. A549 cells with knockdown of NUP58 were injected via tail vein, and the fluorescence images were analyzed. B. A549 cells with knockdown of control were injected via tail vein, and the fluorescence images were analyzed. C. The average radiant efficiency of xenograft tumors in nude mice shows that the intensity of fluorescence in the NC group was higher than in the KD group ($P < 0.01$). D. The numbers of lung metastases were 450 in control group and 24 in knockdown group. E. The numbers of liver metastases were 0 in the control group and 0 in knockdown group.

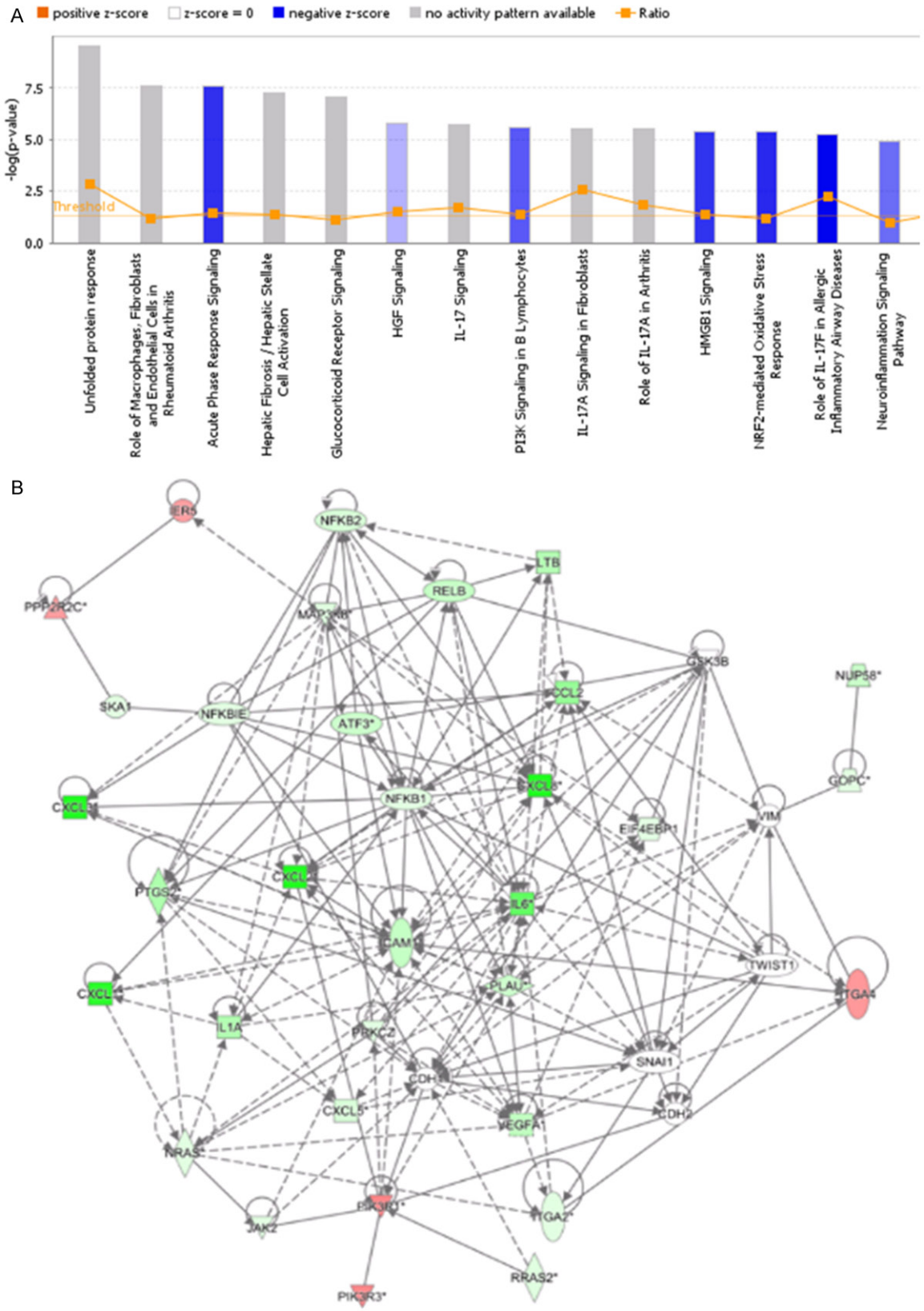

Figure 4. Affymetrix gene expression profile and IPA analysis. A. Gene chip detection shows the significant enrichment of differential genes in classical pathways. The blue annotation indicates that the path is suppressed (z-score < 0). In our study, the PI3K-AKT signaling pathway in the KD group was significantly inhibited, and the Z-score was -3.207. B. Gene co-expression network analyses show a network of interactions between molecules in a defined functional area.

pressed to a lower extent in the KD group than in the NC group. Conversely, E-cadherin was more highly expressed in the KD group than the NC group (**Figure 5C**).

Discussion

Tumor metastasis has long been thought to be the last event of a multistep process, but recent studies have suggested that the seeding of tumor cells can occur even at early stages [16]. The possible reason may be that precancerous cells stimulated by various factors in tumor microenvironment undergo EMT and then acquire the phenotype of infiltration and metastasis [17]. This trait is the basis for a linear pattern of single tumor cell metastasis [18]. In our study, tissue microarrays suggested that NUP58 expression was significantly higher in the tumor cytoplasm or metastatic lesions than in adjacent tissues or primary lesions ($P < 0.05$). The protein levels of NUP58 were also identified by Western Blot in 4 lung adenocarcinoma cell lines (**Figure 1C**). Interestingly, NUP58 expression was higher in 95D and H1299 cell lines than in A549 and 1975 cell lines, the former of which are metastatic cell lines. NUP58 was first reported in the nuclear-pore complex (NPC) structure, which is a complex tunnel that connects the nucleus and cytoplasm and is composed of a variety of nuclear pore proteins. The inner, outer and central parts of the tunnel are composed of ribose nuclear protein, which contribute to these transportation functions [12]. There are no relevant reports about the metastatic function of NUP58 in human lung cancers. Our studies suggested that NUP58 can facilitate metastasis and invasion of lung adenocarcinoma.

The hallmarks of tumor cells are extremely sophisticated, and the present features include: 1. Sustaining proliferative signaling; 2. Evading growth suppressors; 3. Resisting cell death; 4. Enabling replicative immortality; 5. Inducing angiogenesis; 6. Activating invasion and metastasis; 7. Reprogramming energy metabolism; and 8. Avoiding immune destruction [19]. In the process of metastasis and colonization, tumor cells must first have the ability of invasion and then survive under the influence of various factors in microenvironment to finally form metastasis foci in distant tissues [4]. In our study, we found increase in epithelial marker (E-cadherin) and decrease in interstitial marker (N-cadherin) expression with NUP58 knockdown in vitro, which weakened lung cancer cell invasion and metastasis. However, these changes further affected the intravasation of cancer cells into the circulatory system and extravasation through vascular walls into distant tissues in vivo. Currently, the metastasis experiments of xenograft tumors in nude mice have confirmed that the tumor cells can be directly seeded and metastatic at early stages [20]. The mechanism was further clarified in other studies: in the early stage of primary tumors, the metastatic and stem cell like cells accounted for the majority and in the later stages of tumor growth, the cells were mainly hyperplasia cells [21]. However, tumor metastasis may occur many years after malignant transformation, suggesting that there are still many unknown aspects of the tumor metastasis to be elucidated [22].

The molecular features of the EMT process include increased interstitial protein (N-cadherin, vimentin, fibronectin) expression and the loss of epidermal-derived proteins (EpCAM, E-cadherin, cytokeratins, zonula occludins), which are regulated by EMT transcriptional factors and associated signaling pathways [23]. The transcriptional factors and associated signaling pathways (Twist, Snail, ZEB1, PI3K/AKT, etc.) can also be markers of EMT. Our study indicated that Snail, Twist, GSK-3β and phosphorylated GSK-3β (ser9) were significantly lowly expressed except for vimentin after knockdown of NUP58 in an A549 cell line. qPCR results revealed that inhibitors of the PI3K/AKT signaling pathway, including NRAS, NFKBIE, JAK2, PRKCZ, EIF4EBP1, RRAS2, MAP3K8, and PTGS2, were expressed to a lower extent in the KD group than in the NC group ($P < 0.05$). The PI3K/AKT signaling pathway is widely involved in various cellular signal transduction processes, and it plays an important role in cell proliferation [24], apoptosis and energy metabolism in lung cancer [25]. PI3K, AKT, mTOR, p70s6k and other signaling molecules are targets of drug therapy and have been used in clinical patients [26, 27]. It is suggested that NUP58 can promote EMT in lung adenocarcinoma. The underlying mechanism may be partially attributed to inhibition of the GSK-3β signaling pathway. Current studies have found that abnormal activation of GSK-3β in a variety of tumors is closely related to the survival, proliferation and invasion of tumor cells [28]. GSK-3β itself can be either a tumor-promoting factor or a tumor-suppressing factor [29], so it is a promising target for tumor therapy [30]. Previous studies have indicated that Snail is a substrate of GSK-

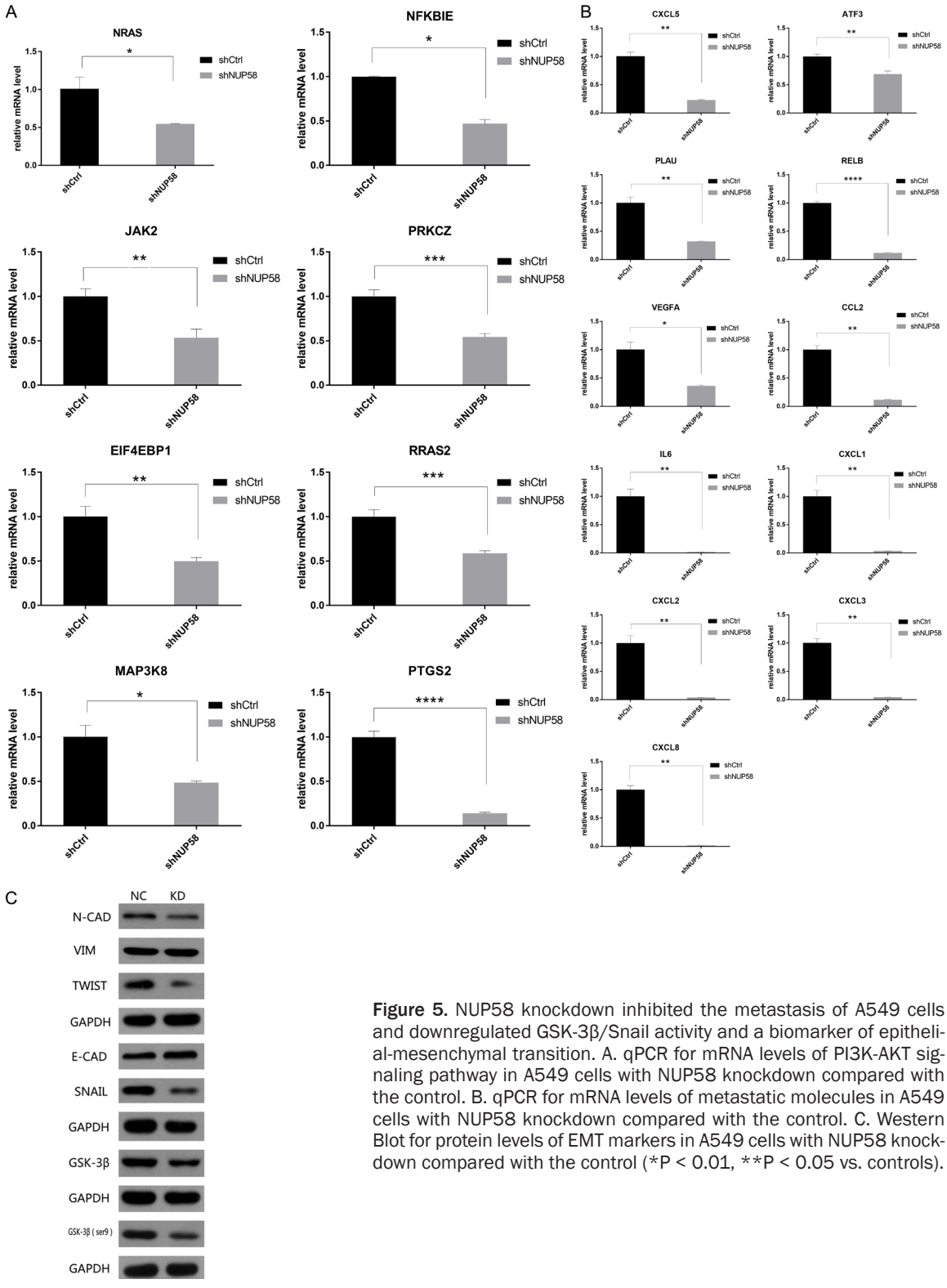

Figure 5. NUP58 knockdown inhibited the metastasis of A549 cells and downregulated GSK-3β/Snail activity and a biomarker of epithelial-mesenchymal transition. A. qPCR for mRNA levels of PI3K-AKT signaling pathway in A549 cells with NUP58 knockdown compared with the control. B. qPCR for mRNA levels of metastatic molecules in A549 cells with NUP58 knockdown compared with the control. C. Western Blot for protein levels of EMT markers in A549 cells with NUP58 knockdown compared with the control (*P < 0.01, **P < 0.05 vs. controls).

3β. Activated PI3K/AKT or MAPK or Wnt pathways can inhibit GSK-3β (through phosphorylation of Ser9), resulting in rescue of Snail, which is inhibited by GSK-3β. Then, Snail triggers the EMT process in tumors. When such pathways are blocked, suppression of GSK-3β is released, which correlates with downregulation of Snail [31, 32]. Similar results were obtained in our

studies: GSK-3β Ser9 phosphorylation (inactive form) and Snail were decreased by knockdown of NUP58, which indicated suppression of Snail by GSK-3β was released. The main function of vimentin in EMT is as one of the components of the middle filament, which can promote the reconstruction of the tumor cell cytoskeleton, form spindle-like shape and facilitate tumor cell metastasis [33]. There is no difference in vimentin expression in our experiment, and it is suggested that the NUP58 gene cannot promote the formation of a spindle-like shape in tumor cells.

Increasing research suggests that tumor metastasis is a result between tumor cells and tumor microenvironment. Neutrophil cells in the tumor microenvironment can not only play the role of immunosuppression but can also help circulating tumor cells to invade endothelial cells [34]. This process depends on the recruitment of neutrophils by the chemokine CCL2 [35] and alteration of vascular endothelial permeability by VEGF [36]. ICAM-1, a kind of intercellular adhesion molecule, is highly expressed in inflammatory diseases and tumors, suggesting that it can promote infiltration of leukocytes, monocytes and tumor molecules around the tissue [37]. Our study suggested the expression of metastatic and invasive factors (ATF3, PLAU, NUP58, RELB, ICAM1, VEGFA, CCL2, IL6, CXCL1, CXCL2, CXCL3, CXCL5, CXCL8) were lower in the KD group than in the NC group ($P < 0.05$). Our study can prove that NUP58 promotes the invasion of lung adenocarcinoma cells.

Conclusions

The NUP58 gene can facilitate metastasis and invasion of lung adenocarcinoma, possibly by activating the AKT-GSK-3β pathway. NUP58 was highly expressed in the primary and metastatic foci of lung adenocarcinoma, with low expression in normal lung tissue and adjacent tissues. In patients with lung adenocarcinoma, the NUP58 gene was highly expressed in patients with stage IV disease.

Acknowledgements

The present study was supported by the Health and Family Planning Commission of Yunnan Province (2016IV5315).

Disclosure of conflict of interest

None.

Abbreviations

NPC, nuclear pore complex; LUAD, lung adenocarcinoma; EMT, epithelial-mesenchymal transition.

Address correspondence to: Jianlin Shi, Department of Thoracic Surgery, Yan'an Affiliated Hospital of Kunming Medical University, 245 East Renmin Road, Kunming 650051, China. E-mail: sjl1984@foxmail.com

References

[1] Siegel RL, Miller KD and Jemal A. Cancer statistics, 2017. CA Cancer J Clin 2017; 67: 7-30.

[2] Chen W, Zhang S and Zou X. [Estimation and projection of lung cancer incidence and mortality in China]. Zhongguo Fei Ai Za Zhi 2010; 13: 488-493.

[3] Pisters KM, Vallieres E, Crowley JJ, Franklin WA, Bunn PA Jr, Ginsberg RJ, Putnam JB Jr, Chansky K and Gandara D. Surgery with or without preoperative paclitaxel and carboplatin in early-stage non-small-cell lung cancer: Southwest Oncology Group Trial S9900, an intergroup, randomized, phase III trial. J Clin Oncol 2010; 28: 1843-1849.

[4] Lambert AW, Pattabiraman DR and Weinberg RA. Emerging biological principles of metastasis. Cell 2017; 168: 670-691.

[5] Paget S. The distribution of secondary growths in cancer of the breast. Cancer Metastasis Rev 1989; 8: 98-101.

[6] Valastyan S and Weinberg RA. Tumor metastasis: molecular insights and evolving paradigms. Cell 2011; 147: 275-292.

[7] Thiery JP. Epithelial-mesenchymal transitions in tumour progression. Nature Reviews Cancer 2002; 2: 442-454.

[8] Yang J and Weinberg RA. Epithelial-mesenchymal transition: at the crossroads of development and tumor metastasis. Dev Cell 2008; 14: 818-829.

[9] Kalluri R and Weinberg RA. The basics of epithelial-mesenchymal transition. J Clin Invest 2009; 119: 1420.

[10] Thiery JP, Acloque H, Huang RY and Nieto MA. Epithelial-mesenchymal transitions in development and disease. Cell 2009; 139: 871-890.

[11] De Craene B and Berx G. Regulatory networks defining EMT during cancer initiation and progression. Nature Reviews Cancer 2013; 13: 97-110.

[12] Meier E, Miller BR and Forbes DJ. Nuclear pore complex assembly studied with a biochemical assay for annulate lamellae formation. J Cell Biol 1995; 129: 1459-1472.

[13] Camps J, Pitt JJ, Emons G, Hummon AB, Case CM, Grade M, Jones TL, Nguyen QT, Ghadimi BM, Beissbarth T, Difilippantonio MJ, Caplen

NJ and Ried T. Genetic amplification of the NOTCH modulator LNX2 upregulates the WNT/beta-catenin pathway in colorectal cancer. Cancer Res 2013; 73: 2003-2013.
[14] Li Y, Xu J, Xiong H, Ma Z, Wang Z, Kipreos ET, Dalton S and Zhao S. Cancer driver candidate genes AVL9, DENND5A and NUPL1 contribute to MDCK cystogenesis. Oncoscience 2014; 1: 854-865.
[15] Zhang W, Luo J, Chen F, Yang F, Song W, Zhu A and Guan X. BRCA1 regulates PIG3-mediated apoptosis in a p53-dependent manner. Oncotarget 2015; 6: 7608-7618.
[16] Hüsemann Y, Geigl JB, Schubert F, Musiani P, Meyer M, Burghart E, Forni G, Eils R, Fehm T and Riethmüller G. Systemic spread is an early step in breast cancer. Cancer Cell 2008; 13: 58-68.
[17] Rhim AD, Mirek ET, Aiello NM, Maitra A, Bailey JM, McAllister F, Reichert M, Beatty GL, Rustgi AK and Vonderheide RH. EMT and dissemination precede pancreatic tumor formation. Cell 2012; 148: 349-361.
[18] Turajlic S and Swanton C. Metastasis as an evolutionary process. Science 2016; 352: 169-175.
[19] Hanahan D and Weinberg RA. Hallmarks of cancer: the next generation. Cell 2011; 144: 646-674.
[20] Weng D, Penzner JH, Song B, Koido S, Calderwood SK and Gong J. Metastasis is an early event in mouse mammary carcinomas and is associated with cells bearing stem cell markers. Breast Cancer Res 2012; 14: R18.
[21] Hosseini H, Obradović MM, Hoffmann M, Harper KL, Sosa MS, Werner-Klein M, Nanduri LK, Werno C, Ehrl C and Maneck M. Early dissemination seeds metastasis in breast cancer. Nature 2016; 540: 552-558.
[22] Yachida S, Jones S, Bozic I, Antal T, Leary R, Fu B, Kamiyama M, Hruban RH, Eshleman JR and Nowak MA. Distant metastasis occurs late during the genetic evolution of pancreatic cancer. Nature 2010; 467: 1114-1117.
[23] Jie XX, Zhang XY and Xu CJ. Epithelial-to-mesenchymal transition, circulating tumor cells and cancer metastasis: mechanisms and clinical applications. Oncotarget 2017; 8: 81558.
[24] Porta C, Paglino C and Mosca A. Targeting PI3K/Akt/mTOR signaling in cancer. Front Oncol 2014; 4: 64.
[25] Guerriero I, D'Angelo D, Pallante P, Santos M, Scrima M, Malanga D, De Marco C, Weisz A, Laudanna C and Ceccarelli M. Analysis of miRNA profiles identified miR-196a as a crucial mediator of aberrant PI3K/AKT signaling in lung cancer cells. Oncotarget 2017; 8: 19172.
[26] Fang Y, Zhang C, Wu T, Wang Q, Liu J and Dai P. Transcriptome sequencing reveals key pathways and genes associated with cisplatin resistance in lung adenocarcinoma A549 cells. PLoS One 2017; 12: e0170609.
[27] Jiang J, Feng X, Zhou W, Wu Y and Yang Y. MiR-128 reverses the gefitinib resistance of the lung cancer stem cells by inhibiting the c-met/PI3K/AKT pathway. Oncotarget 2016; 7: 73188.
[28] Domoto T, Pyko IV, Furuta T, Miyashita K, Uehara M, Shimasaki T, Nakada M and Minamoto T. Glycogen synthase kinase-3beta is a pivotal mediator of cancer invasion and resistance to therapy. Cancer Sci 2016; 107: 1363-1372.
[29] McCubrey JA, Davis NM, Abrams SL, Montalto G, Cervello M, Basecke J, Libra M, Nicoletti F, Cocco L, Martelli AM and Steelman LS. Diverse roles of GSK-3: tumor promoter-tumor suppressor, target in cancer therapy. Adv Biol Regul 2014; 54: 176-196.
[30] McCubrey JA, Steelman LS, Bertrand FE, Davis NM, Sokolosky M, Abrams SL, Montalto G, D'Assoro AB, Libra M, Nicoletti F, Maestro R, Basecke J, Rakus D, Gizak A, Demidenko ZN, Cocco L, Martelli AM and Cervello M. GSK-3 as potential target for therapeutic intervention in cancer. Oncotarget 2014; 5: 2881-2911.
[31] Lan Y, Han J, Wang Y, Wang J, Yang G, Li K, Song R, Zheng T, Liang Y, Pan S, Liu X, Zhu M, Liu Y, Meng F, Mohsin M, Cui Y, Zhang B, Subash S and Liu L. STK17B promotes carcinogenesis and metastasis via AKT/GSK-3beta/Snail signaling in hepatocellular carcinoma. Cell Death Dis 2018; 9: 236.
[32] Zhou BP, Deng J, Xia W, Xu J, Li YM, Gunduz M and Hung MC. Dual regulation of Snail by GSK-3beta-mediated phosphorylation in control of epithelial-mesenchymal transition. Nat Cell Biol 2004; 6: 931-940.
[33] Satelli A and Li S. Vimentin in cancer and its potential as a molecular target for cancer therapy. Cell Mol Life Sci 2011; 68: 3033-46.
[34] Coffelt SB, Wellenstein MD and de Visser KE. Neutrophils in cancer: neutral no more. Nat Rev Cancer 2016; 16: 431-446.
[35] Qian BZ, Li J, Zhang H, Kitamura T, Zhang J, Campion LR, Kaiser EA, Snyder LA and Pollard JW. CCL2 recruits inflammatory monocytes to facilitate breast-tumour metastasis. Nature 2011; 475: 222-225.
[36] Qian B, Deng Y, Im JH, Muschel RJ, Zou Y, Li J, Lang RA and Pollard JW. A distinct macrophage population mediates metastatic breast cancer cell extravasation, establishment and growth. PLoS One 2009; 4: e6562.
[37] Liou CJ and Huang WC. Casticin inhibits interleukin-1beta-induced ICAM-1 and MUC5AC expression by blocking NF-kappaB, PI3K-Akt, and MAPK signaling in human lung epithelial cells. Oncotarget 2017; 8: 101175-101188.

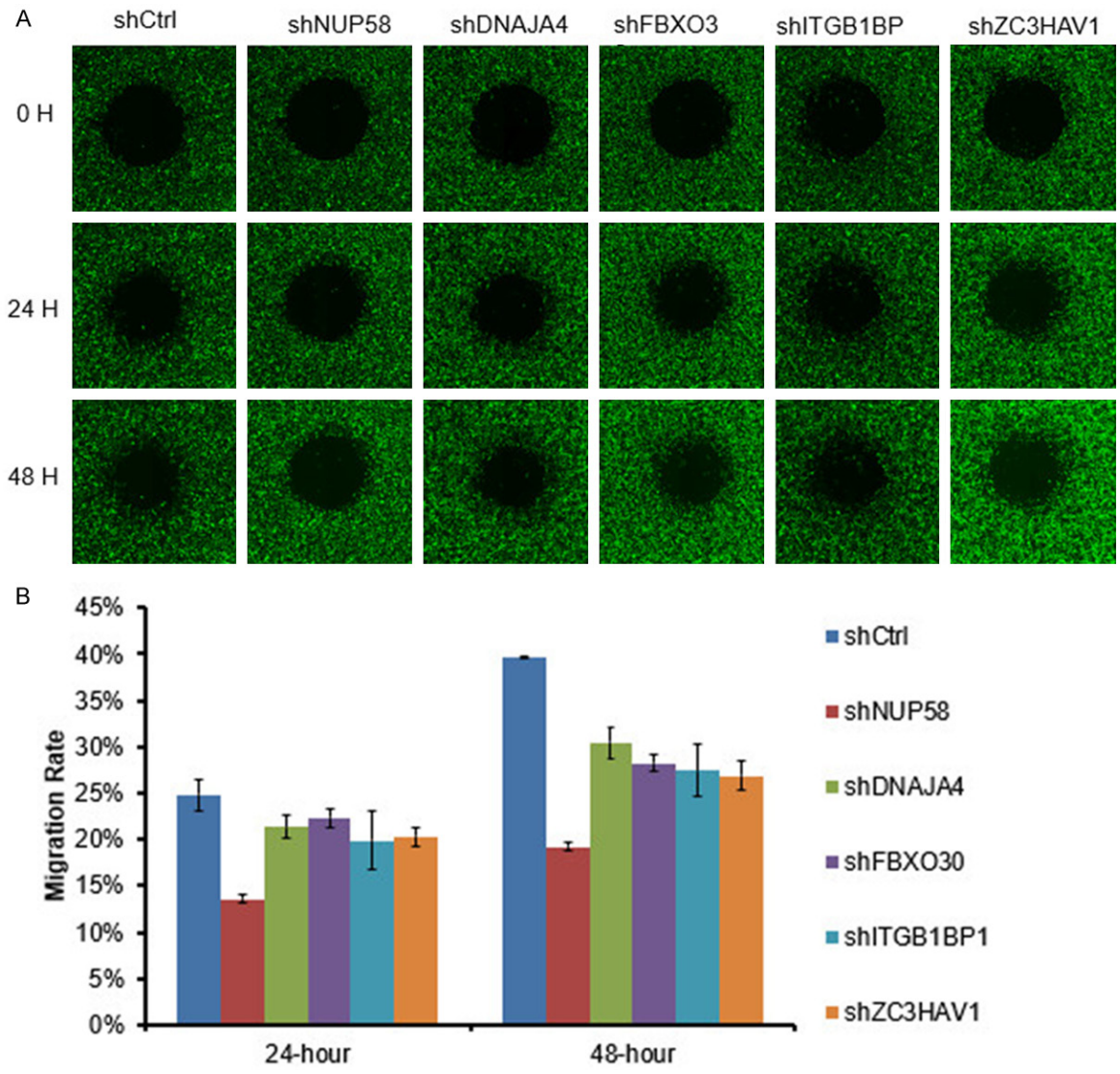

Supplementary Figure 1. Previous works of screening metastatic target of LUAD.

Supplementary Table 1. Primer list for qPCR

Target gene	Upstream primer sequence	Downstream primer sequence	size
NRAS	TGAAACCTCAGCCAAGACCAG	TGGCAATCCCATACAACCCT	130
PIK3R1	ACCACTACCGGAATGAATCTCT	GGGATGTGCGGGTATATTCTTC	207
NFKBIE	TTACCCATGTTGGGTCAGCC	AACGGTGTTTCAGGGTCCTC	140
ITGA2	CCTACAATGTTGGTCTCCCAGA	AGTAACCAGTTGCCTTTTGGATT	106
JAK2	ATCCACCCAACCATGTCTTCC	ATTCCATGCCGATAGGCTCTG	121
NFKB2	TCCGATTTCGATATGGCTGTG	CTTGGCTGGTCCCTCGTAGTT	110
NFKB1	AGGATTTCGTTTCCGTTATGT	CCTGAGGGTAAGACTTCTTGTTC	92
PRKCZ	CTTACATTTCCTCATCCCGGAAG	TTCACCACTTTCATGGCGTAAA	214
EIF4EBP1	GATCTGCCCACCATTCCG	CCGCCCGCTTATCTTCTG	103
PIK3R3	AAAGGAGTGAGACAGAAACGC	CCACAGAGCAAGCATAGCATC	232
RRAS2	GCATCAGCAAAGATTAGGA	TGGTTCTGGTGAAGGAGGA	102
PPP2R2C	TTACCGAACGAGATAAAAGGC	TGTTGACGGAGATGGAGTTG	189
MAP3K8	TGTTCAAATGACCGAAGATG	ACAGGTAGGAGGGATAGGCT	200
PTGS2	CTCCTGTGCCTGATGATTGC	CAGCCCGTTGGTGAAAGC	215
ITGA4	AGTTGGTGCTTTTCGGTCT	TGCCTTTCTGTTCACATCC	235
CXCL5	CAGACCACGCAAGGAGTT	CTTCAGGGAGGCTACCAC	99
ATF3	GCTAAGCAGTCGTGGTATG	CTGGAGTTGAGGCAAAGAT	225
PLAU	CTGTCACCTACGTGTGTGGAG	TGAGCGACCCAGGTAGACG	116
NUP58	AGGTATTGGCACTGGCTTGC	CTTCCTGAGGGTTTATTTGTTG	138
RELB	CAGCCTCGTGGGGAAAGAC	CCAGCGTTGTAGGGGTCAA	171
ICAM1	CAAGAAGATAGCCAACCAATG	GCCAGTTCCACCCGTTC	104
VEGFA	AACTTTCTGCTGTCTTGGGT	TCTCGATTGGATGGCAGTA	166
LTB	CTGGGAGACGACGAAGGAACA	GCCGACGAGACAGTAGAGGTA	112
IL1A	AGATGCCTGAGATACCCAAAACC	CCAAGCACACCCAGTAGTCT	147
CCL2	CAGCCAGATGCAATCAATGCC	TGGAATCCTGAACCCACTTCT	190
IL6	CAAATTCGGTACATCCTCG	CTCTGGCTTGTTCCTCACTA	259
CXCL1	AAACCGAAGTCATAGCCACA	CCTAAGCGATGCTCAAACA	247
CXCL2	CCAAACCGAAGTCATAGC	GAACAGCCACCAATAAGC	150
CXCL3	CGCCCAAACCGAAGTCATAG	GCTCCCCTTGTTCAGTATCTTTT	109
CXCL8	TGGCAGCCTTCCTGATTT	AACCCTCTGCACCCAGTT	236

Supplementary Table 2. Clinical features of cohort 1

Clinical featrues	Number	Chi-Square	*P* value
Age		1.863	0.172
≤ 65 years	57 (61.96%)		
> 65 years	35 (38.04%)		
Sex			
Male	51 (55.43%)	1.777	0.183
Female	41 (44.57%)		
Pathological grade		2.779	0.249
I stage	1 (1.09%)		
II stage	56 (60.87%)		
III stage	35 (38.04%)		
Tumor size		1.636	0.201
≤ 5 cm	67 (84.81%)		
> 5 cm	12 (15.19%)		
T stage		8.916	0.03
T1	23 (29.11%)		
T2	37 (46.84%)		
T3	12 (15.19%)		
T4	7 (8.86%)		
N stage		3.878	0.275
N0	34 (62.96%)		
N1	13 (24.07%)		
N2	6 (11.11%)		
N3	1 (1.85%)		
M stage		1.784	0.182
M0	90 (97.83%)		
M1	2 (2.17%)		
TNM stage			
TNM I	25 (37.31%)	7.788	0.051
TNM II	21 (31.34%)		
TNM III	19 (28.36%)		
TNM IV	2 (2.99%)		

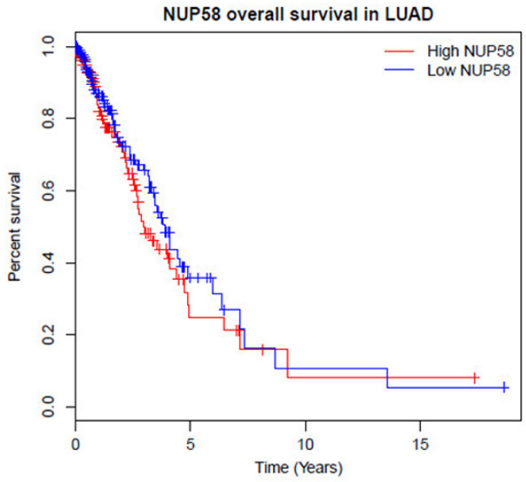

Supplementary Figure 2. Survival of NUP58 in LUAD patients.

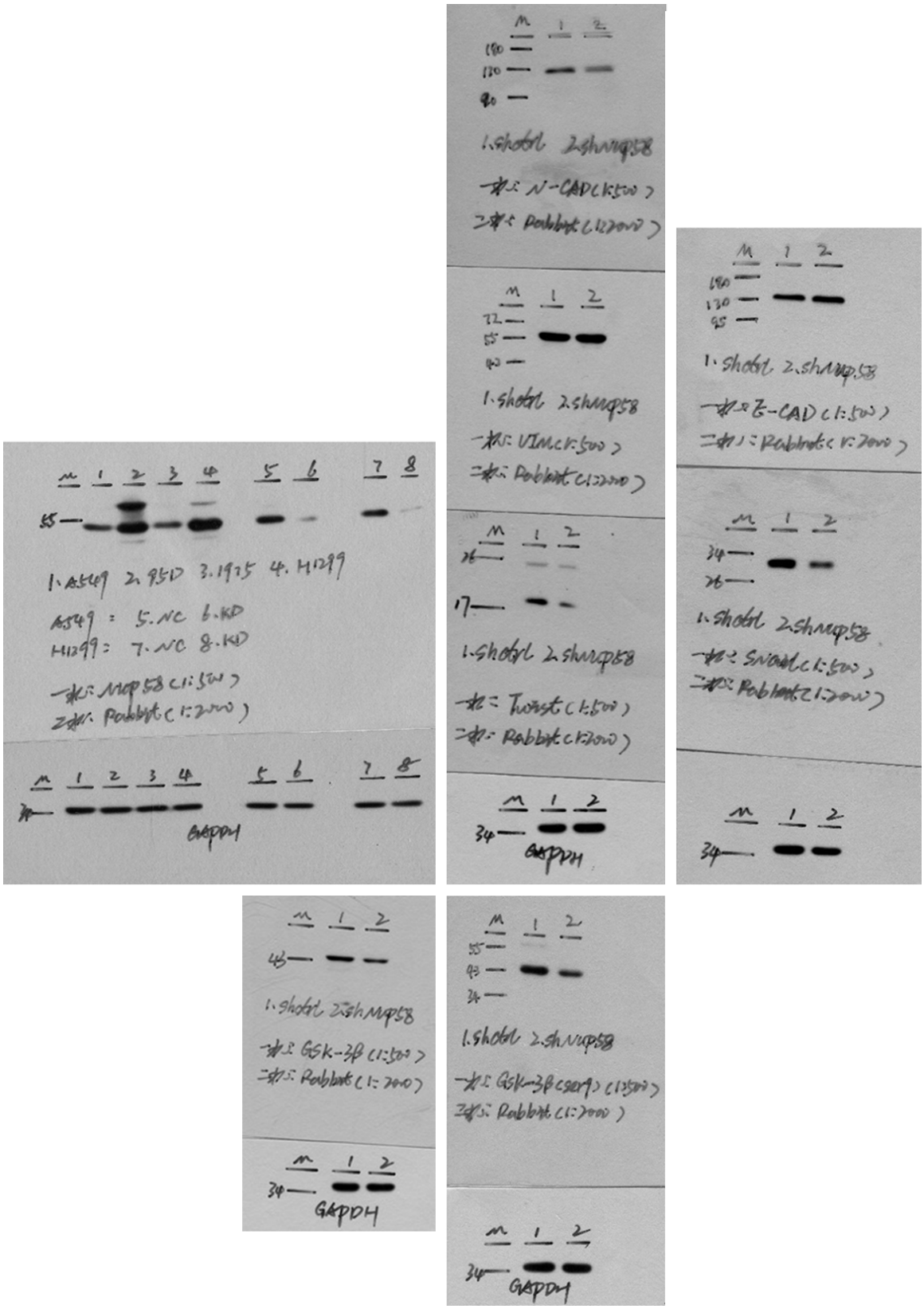

Supplementary Figure 3. Original western blot images.